Toxicology Reports 2 (2015) 1281–1290

Contents lists available at ScienceDirect

Toxicology Reports

journal homepage: www.elsevier.com/locate/toxrep

Effects of 3-styrylchromones on metabolic profiles and cell death in oral squamous cell carcinoma cells

Hiroshi Sakagami[a,*], Chiyako Shimada[a], Yumiko Kanda[b], Osamu Amano[c], Masahiro Sugimoto[d], Sana Ota[d], Tomoyoshi Soga[d], Masaru Tomita[d], Akira Sato[e], Sei-ichi Tanuma[e], Koichi Takao[f], Yoshiaki Sugita[f]

[a] Division of Pharmacology, Meikai University School of Dentistry, Sakado, Saitama, Japan
[b] Department of Electron Microscope, Meikai University School of Dentistry, Sakado, Saitama, Japan
[c] Division of Anatomy, Meikai University School of Dentistry, Sakado, Saitama, Japan
[d] Institute for Advanced Bioscience, Keio University, Tsuruoka, Yamagata, Japan
[e] Department of Biochemistry, Faculty of Pharmaceutical Sciences, Tokyo University of Science, Noda, Chiba, Japan
[f] Faculty of Pharmaceutical Sciences, Josai University, Sakado, Saitama, Japan

ARTICLE INFO

Article history:
Received 7 July 2015
Received in revised form
19 September 2015
Accepted 26 September 2015

Chemical compounds studied in this article:
Chromone (PubChem CID: 10286)
2-Styrylchromone (PubChem CID: 754332)
Doxorubicin (PubChem CID: 31703)
5-Fluorouracil (5-FU) (PubChem CID: 3385)
3-(4,5-Dimethylthiazol-2-yl)-2,5-diphenyltetrazolium bromide (PubChem CID: 64965)
Diethanolamine (PubChem CID: 8113)
Choline (PubChem CID: 305)
CDP-choline (PubChem CID: 25202509)
D-Mannitol (PubChem CID: 6251)

Keywords:
3-Styrylchromones
Cytotoxicity
Mitochondria
Metabolomics profiling
Apoptosis
Autophagy

ABSTRACT

4*H*-1-benzopyran-4-ones (chromones) are important naturally-distributing compounds. As compared with flavones, isoflavones and 2-styrylchromones, there are only few papers of 3-styrylchromones that have been published. We have previously reported that among fifteen 3-styrylchromone derivatives, three new synthetic compounds that have OCH_3 group at the C-6 position of chromone ring, (*E*)-3-(4-hydroxystyryl)-6-methoxy-4*H*-chromen-4-one (compound **11**), (*E*)-6-methoxy-3-(4-methoxystyryl)-4*H*-chromen-4-one (compound **4**), (*E*)-6-methoxy-3-(3,4,5-trimethoxystyryl)-4*H*-chromen-4-one (compound **6**) showed much higher cytotoxicities against four epithelial human oral squamous cell carcinoma (OSCC) lines than human normal oral mesenchymal cells. In order to further confirm the tumor specificities of these compounds, we compared their cytotoxicities against both human epithelial malignant and non-malignant cells, and then investigated their effects on fine cell structures and metabolic profiles and cell death in human OSCC cell line HSC-2. Cytotoxicities of compounds **4**, **6**, **11** were assayed with MTT method. Fine cell structures were observed under transmission electron microscope. Cellular metabolites were extracted with methanol and subjected to CE-TOFMS analysis. Compounds **4**, **6**, **11** showed much weaker cytotoxicity against human oral keratinocyte and primary human gingival epithelial cells, as compared with HSC-2, confirming their tumor-specificity, whereas doxorubicin and 5-FU were highly cytotoxic to these normal epithelial cells, giving unexpectedly lower tumor-specificity. The most cytotoxic compound **11**, induced the mitochondrial vacuolization, autophagy suppression followed by apoptosis induction, and changes in the metabolites involved in amino acid and glycerophospholipid metabolisms. Chemical modification of lead compound **11** may be a potential choice for designing new type of anticancer drugs.

1. Introduction

4*H*-1-benzopyran-4-ones (chromones) are an important class of oxygenated heterocyclic compounds since the chromone core structure is found in flavones, isoflavones and 2-styrylchromones. As compared with flavones and isoflavones, 2-styrylchromones constitute a much smaller group of naturally occurring chromones. Synthetic 2-styrylchromones showed antioxidant [1], anti-allergic [2], anti-inflammatory [3], antitumor [4–6], and antiviral [7,8] activities. In contrast, as far as we know there were only two papers of 3-styrylchromones that investigated the antiviral [9] and antibacterial activities [10]. We have recently synthesized a series of 3-styrylchromone derivatives, with antioxidant and α-glycosidase inhibition activities [11], and

* Corresponding author. Fax: +81 49 285 5171.
E-mail address: sakagami@dent.meikai.ac.jp (H. Sakagami).

http://dx.doi.org/10.1016/j.toxrep.2015.09.009

Table 1
Cytotoxicity of 3-styrylchromones against human oral squamous cell carcinoma and various oral normal cells. The data of Ca9-22, HSC-2, HSC-3, HSC-4, HGF, HPLF and HPC were cited from Ref. [12].

		3-Styrylchromones			Positive controls	
Target cells		[4]	[6]	[11]	Doxorubicin	5-FU
Human oral squamous cell carcinoma	50% cytotoxic concentration (CC_{50}) (μM)					
Derived from gingiva (Ca9-22)	A	4.4	10	2.1	0.26	29
Derived from tongue (HSC-2)		4.4	6.8	1.0	0.12	13
Derived from tongue (HSC-3)		7.7	21	3.6	0.11	16
Derived from tonuge (HSC-4)		9.2	13	1.2	0.094	13
Average (mean ± S.D.)	B	6.4 ± 2.4	13 ± 6.1	2.0 ± 1.2	0.15 ± 0.077	18 ± 7.6
Human norml oral cells						
Gingival fibroblast (HGF) (C)	C	229	544	67	0.87	>1000
Periodonal ligament fibroblast (HPLF)		150	190	74	0.87	>1000
Pupl cell (HPC)		396	284	272	>10	>1000
Average (mean)	D	258 ± 126	339 ± 183	138 ± 116	>3.9 ± 5.3	>1000
Oral keratinocyte (HOK)	E	70	77	19	1.31	24.7
Primary gingival epithelial cell (HGEP)	F	178	610	>800	0.027	18.8
	Tumor-specificity index (TS)					
	D/B	40.3	26.1	69.0	>26.0	>55.6
	C/A	52.0	54.4	31.9	3.3	>34.5
	E/B	10.9	5.9	9.5	8.7	1.4
	F/B	27.8	46.9	>400	0.2	1.0
	$PSE = TS \times (1/B) \times 100$					
	D/B^2	630	200	3450	>17333	>309
	E/B^2	170	45	475	5800	7.8
	F/B^2	434	361	>20000	133	5.6

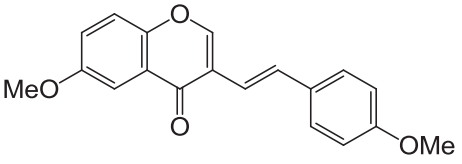

(*E*)-6-Methoxy-3-(4-methoxystyryl)-4*H*-chromen-4-one [**4**]

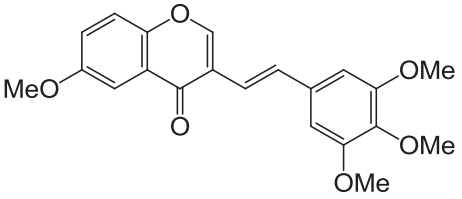

(*E*)-6-Methoxy-3-(3,4,5-trimethoxystyryl)-4*H*-chromen-4-one [**6**]

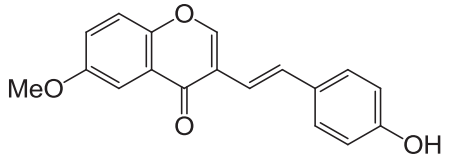

(*E*)-3-(4-Hydroxystyryl)-6-methoxy-4*H*-chromen-4-one [**11**]

Fig. 1. Structure of (*E*)-6-methoxy-3-(4-methoxystyryl)-4*H*-chromen-4-one (compound **4**), (*E*)-6-methoxy-3-(3,4,5-trimethoxystyryl)-4*H*-chromen-4-one (compound **6**) and (*E*)-3-(4-hydroxystyryl)-6-methoxy-4*H* -chromen-4-one (compound **11**).

reported tumor-specific cytotoxicity [12]. Among fifteen 3-styrylchromones, three new synthetic compounds that have a methoxy group at 6-position of the chromone ring, (*E*)-3-(4-hydroxystyryl)-6-methoxy-4*H*-chromen-4-one (compound **11**), (*E*)-6-methoxy-3-(4-methoxystyryl)-4*H*-chromen-4-one (compound **4**), (*E*)-6-methoxy-3-(3,4,5-trimethoxystyryl)-4*H*-chromen-4-one (compound **6**) (Fig. 1) showed much higher cytotoxicities against four human oral squamous cell lines [Ca9-22 (derived from gingiva), HSC-2, HSC-3, and HSC-4 (derived from tongue)] than against human normal oral mesenchymal cells [gingival fibroblast (HGF), periodontal ligament fibroblast (HPLF), and pulp cell (HPC)] (cited from Ref. [12] and shown in the upper part of Table 1). The tumor-specificity (TS), determined as the ratio of mean CC_{50} for human normal cells to that for human oral squamous cell carcinoma cell (D/B in Table 1) (TS = 40.3, 26.1, 69.0) was comparable with that for popular anti-cancer drugs, doxorubicin and 5-FU (TS >26, >55.6). 3-Styrylchromones (compounds **4**, **6**, **11**) and 5-FU showed much higher cytotoxicity against Ca9-22 cells than HGF cells (both derived from gingival tissues), giving higher TS values as compared with doxorubicin (52.0, 54.4, 31.9, >34.5 vs. 3.3) (C/A in Table 1). However, these normal cells were derived from mesenchymal tissues, different from epithelial tissue-derived OSCC cell lines.

In the present study, we first investigated the cytotoxicity of these synthetic compounds **4**, **6**, **11** against epithelial human oral keratinocyte (HOK) and primary human gingival epithelial cells (HGEP) to confirm their tumor-specificity. We then determined the minimum treatment time required for cytotoxicity induction by the most active compound **11** in a sensitive human OSCC cell line HSC-2. Metabolomics, the measurement of all intracellular metabolites, has become a powerful tool to gain insight into cellular function and site of action. Therefore, using this technology, we finally investigated possible changes in fine cell structure and type of cell death, and metabolic profiles induced by compound **11**.

2. Materials and method

2.1. Materials

The following chemicals and reagents were obtained from the indicated companies: Dulbecco's modified Eagle's medium (DMEM), from GIBCO BRL, Grand Island, NY, USA; fetal bovine serum (FBS), doxorubicin, 3-(4,5-dimethylthiazol-2-yl)-2,5-diphenyltetrazolium bromide (MTT), tetraethylammonium chloride (TEM) from Sigma–Aldrich Inc., St. Louis, MO, USA; dimethyl sulfoxide (DMSO), cycloheximide from Wako Pure Chem. Ind., Osaka, Japan; 5-fluorouracil (5-FU) from Kyowa, Tokyo, Japan;

culture plastic dishes and plates (96-well) were purchased from Becton Dickinson (Franklin Lakes, NJ, USA).

2.2. Synthesis of test compounds

(*E*)-6-Methoxy-3-(4-methoxystyryl)-4*H*-chromen-4-one (compound **4**), (*E*)-6-methoxy-3-(3,4,5-trimethoxystyryl)-4*H*-chromen-4-one (compound **6**) and (*E*)-3-(4-hydroxystyryl)-6-methoxy-4*H*-chromen-4-one (compound **11**) (Fig. 1) were synthesized by Knoevenagel condensation of the appropriate 3-formylchromone with selected phenylacetic acid derivatives, as described previously [11]. All compounds were characterized by ^{1}H NMR, MS spectra and elemental analyses after purification by silica gel column chromatography and recrystallization. All compounds were dissolved in DMSO at 80 mM and stored at −20 °C before use.

2.3. Cell culture

Human oral normal cells, gingival fibroblast (HGF), periodontal ligament fibroblast (HPLF) and pulp cell (HPC), established from the first premolar tooth extracted from the lower jaw of a 12-year-old girl [13], and OSCC cell lines (Ca9-22, HSC-2, HSC-3, HSC-4), purchased from Riken Cell Bank, Tsukuba, Japan were cultured at 37 °C in DMEM supplemented with 10% heat-inactivated FBS, 100 units/ml, penicillin G and 100 μg/ml streptomycin sulfate under a humidified 5% CO_2 atmosphere. Human oral keratinocytes (HOK) (purchased from COSMO BIO Co./Ltd., Tokyo) was cultured in keratinocyte growth supplement (OKGS, Cat, No. 2652). Primary human gingival epithelial cells (HGEP) (purchased from CELLnTEC Advanced Cell Systems AG, Bern, Switzerland) was growing in CnT-PR medium. Cells were then harvested by treatment with 0.25% trypsin-0.025% EDTA-2Na in PBS(−) and either subcultured or used for experiments.

2.4. Assay for cytotoxic activity

Cells were inoculated at 2.5×10^3 cells/0.1 ml in a 96-microwell plate. After 48 h, the medium was removed by suction with an aspirator and replaced with 0.1 ml of fresh medium containing different concentrations of compound **4**, **6** or **11**, or vehicles that contained the same amounts of DMSO without sample (as control). Usually, DMSO concentration was below 0.0125%. Cells were incubated for the indicated times, and the relative viable cell number was then determined by the MTT method. In brief, the treated cells were incubated for another 3 h in fresh culture medium containing 0.2 mg/ml MTT. Cells were then lysed with 0.1 ml of DMSO and the absorbance at 540 nm of the cell lysate was determined using a microplate reader (Biochromatic Labsystem, Helsinki, Finland). The CC_{50} was determined from the dose–response curve.

2.5. Fine cell structure

HSC-2 cells were inoculated at 5×10^5 cells/10 ml in 10 cm dishes and incubated for 3 h. After medium change, near confluent cells were treated for 3 h with 0 (control), 3 or 10 μM of compound **11**. After washing three times with 5 ml of cold PBS(−), the cells were fixed for 1 h with 2% glutaraldehyde in 0.1 M cacodylate buffer (pH 7.4) at 4 °C. The cells were scraped with a rubber policemen, pelleted by centrifugation, post-fixed for 90 min with 1% osmium tetraoxide-0.1 M cacodylate buffer (pH 7.4), dehydrated and embedded in Araldite M (CIBA-GEIGY Swiss; NISSHIN EN Co., Ltd., Tokyo, Japan). Thin sections were stained with uranyl acetate and lead citrate, and were then observed under a JEM-1210 transmission electron microscope, Japan Electron Optics Laboratory (JEOL, Co., Ltd., Akishima, Tokyo, Japan) (magnification: ×5000) at an accelerating voltage of 100 kV [14].

2.6. Western blot analysis

HSC-2 cells were washed in ice-cold PBS and then whole cell lysates were prepared using laemmli sample buffer. Whole cell lysates (5×10^4 cells per lane) were separated by 12% SDS-polyacrylamide gel electrophoresis, and blotted onto a PVDF membrane (Merck Millipore, Darmstadt, Germany). The membrane was then blocked against non-specific binding by treatment for 1 h with 5% bovine serum albumin in Tris-buffered saline (pH 7.6) containing 0.1% Tween 20, and then immunoblotted overnight at 4 °C using the respective primary antibody. Next, the membrane was incubated for 1 h at room temperature with a horseradish peroxidase-conjugated anti-rabbit IgG secondary antibody, and the protein bands were visualized using an immobilon Western Chemiluminescent HRP Substrate (Merck Millipore). Protein expression was quantified using ChemiDoc MP imaging system (Bio-Rad, Hercules, CA, USA). The following antibodies were used: anti-PARP, anti-caspase 3 antibodies (1:1000, Cell Signaling Technology, Danvers, MA, USA), anti-LC3 antibody (1:1000, Medical & Biological Laboratories, Nagoya, Japan), anti-glyceraldehyde-3-phosphate dehydrogenase (GAPDH) antibody (1:20,000, Trevigen, Helgerman, Gaithersburg, MD, USA), and anti-rabbit IgG horseradish peroxidase-linked whole antibody (1:20,000, GE Healthcare, Little Chalfont, Buckinghamshire, England).

2.7. Processing for metabolomic analysis

HSC-2 cells were inoculated at 5×10^5 cells/10 ml in 10 cm dishes and incubated for 48 h. The medium was replaced with fresh medium and the cells were incubated for 30 min at 37 °C in a 5% CO_2 incubator to stabilize the pH and temperature of the culture medium. The cells were treated for 3 h with 0 (control), 1, 3 and 10 μM of compound **11**. Aliquots of the cells were trypsinized for counting the viable cell number with hemocytometer after staining with trypan blue. The remaining cells were washed twice with 5 ml of ice cold 5 % D-mannitol solution and then immersed for 10 min in 1 ml of methanol containing internal standards (25 μM each of methionine sulfone, 2-[*N*-morpholino]-ethanesulfonic acid and D-camphor-10-sulfonic acid). Cold 5% D-mannitol solution was used to minimize the leak of intracellular metabolites during the washing process, and metabolites were directly extracted with methanol from the attached cells, since detachment of the cells by trypsin resulted in a significant loss of intracellular metabolites [15], and scraping off the cells by a rubber policeman caused 5–10% of cell death (unpublished data). We confirmed that only a few percent of lactate was solubilized from the blank samples in plastic by chloroform treatment, indicating the cross-contamination within the extraction procedure was very little [16], and this blank was subtracted from all samples. The methanol extract (supernatant) was collected. To 400 μl of the dissolved samples, 400 μl of chloroform and 200 μl of Milli-Q water were added and the mixture was centrifuged at 10,000 × *g*, for 3 min at 4 °C. The aqueous layer was filtered to remove large molecules by centrifugation through a 5 kDa cut-off filter (Millipore, Billerica, MA) at 9100 × *g* for 3.0 h at 4 °C. The 320 μl of the filtrate was concentrated by centrifugation and dissolved in 50 μl of Milli-Q water containing reference compounds (200 μM each of 3-aminopyrrolidine and trimesate) immediately before CE-TOFMS analysis [15–18].

All samples were quantified using one-time batch measurement. The sensitivity fluctuation derived from mass spectrometry was corrected by internal standards added to each sample. However, we also confirmed the consistency of the sensitivity among all samples measured in this study, since the

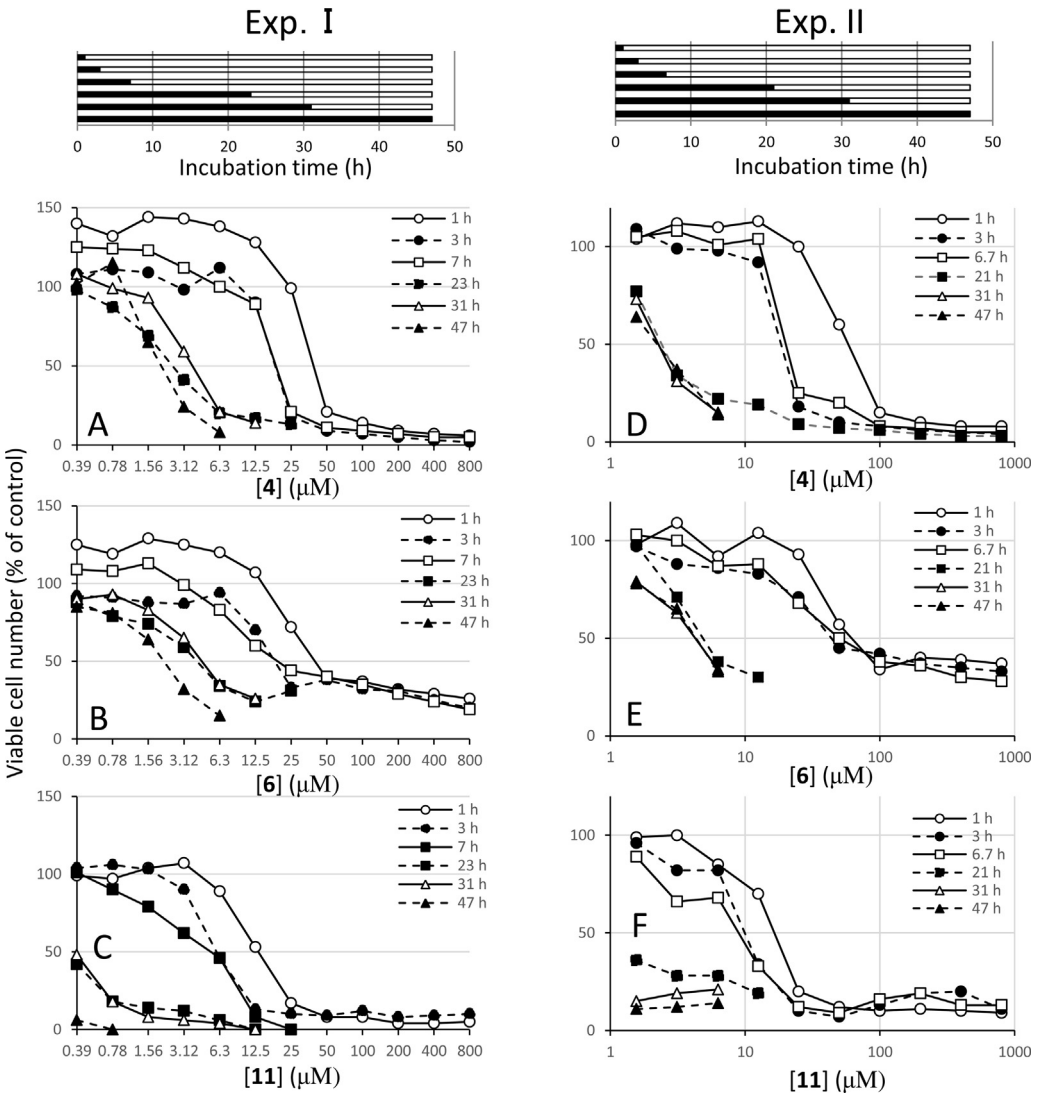

Fig. 2. Time course of cytotoxicity induction by (*E*)-6-methoxy-3-(4-methoxystyryl)-4*H*-chromen-4-one (compound **4**), (*E*)-6-methoxy-3-(3,4,5-trimethoxystyryl)-4*H*-chromen-4-one (compound **6**) and (*E*)-3-(4-hydroxystyryl)-6-methoxy-4*H*-chromen-4-one (compound **11**). HSC-2 cells were incubated for the indicated times, and medium was replaced with fresh medium and incubated further until 47 h after the initial addition of samples. The relative viable cell number was then determined by the MTT method. Each value presents mean of triplicate (Exp. I) and quadruplicate (Exp. II) assays. The difference between control and treated group that shows less than 80% of viability was statistically significant ($p < 0.05$). Two experiments (Exp. I and II) showed similar results. The 50% cytotoxic concentration (CC_{50}) was calculated and listed in Table 1.

peak areas of the internal standards were nearly constant in all measurements. Data of intracellular concentration of each metabolite was presented after normalization by cell count. A targeted assay that detects the peaks at the sample place with commercially available samples [19] was used in the present study.

2.8. Instrument parameters for metabolomic analysis

The instrumentation and measurement conditions used for CE-TOF-MS were described elsewhere [20,21] with slight modification [18]. We used the capillary electrophoresis (CE) among various types of separation systems available for metabolomics profiling, since this method is quantitative, sensitive, and robust, and its utility was demonstrated in the analysis of broader primary pathways whose most metabolites were electronically charged [22], as compared with conventional liquid chromatography (LC) or gas chromatography (GS) that required repeated running due to their narrow analysis range. Cation analysis was performed using an Agilent CE capillary electrophoresis system, an Agilent G6220A LC/MSD TOF system, an Agilent 1100 series isocratic HPLC pump, a G1603A Agilent CEMS adapter kit, and a G1607A Agilent CE-ESI-MS sprayer kit (Agilent Technologies, Waldbronn, Germany). Anion analysis was performed using an Agilent CE capillary electrophoresis system, an Agilent G1969A LC/MSD TOF system, an Agilent 1200 series isocratic HPLC pump, a G1603A Agilent CE-MS adapter kit, and a G7100A Agilent CE-electrospray ionization (ESI) source-MS sprayer kit (Agilent Technologies). For the cation and anion analyses, the CE-MS adapter kit included a capillary cassette that facilitates thermostatic control of the capillary. The CE-ESI-MS sprayer kit simplifies coupling of the CE system with the MS system and is equipped with an electrospray source. For system control and data acquisition, 3D-CE ChemStation software (Rev. B.04.01.SP1) was used for CE. Agilent MassHunter software (B.02.00, B1128.5) and AnalystQS (ver.1.1 Build 9865, Applied Biosystems, Foster, CA) were used for TOF-MS. The original Agilent SST316Ti stainless steel ESI needle was replaced with a passivated SST316Ti stainless steel and platinum needle (passivated with 1% formic acid and a 20%

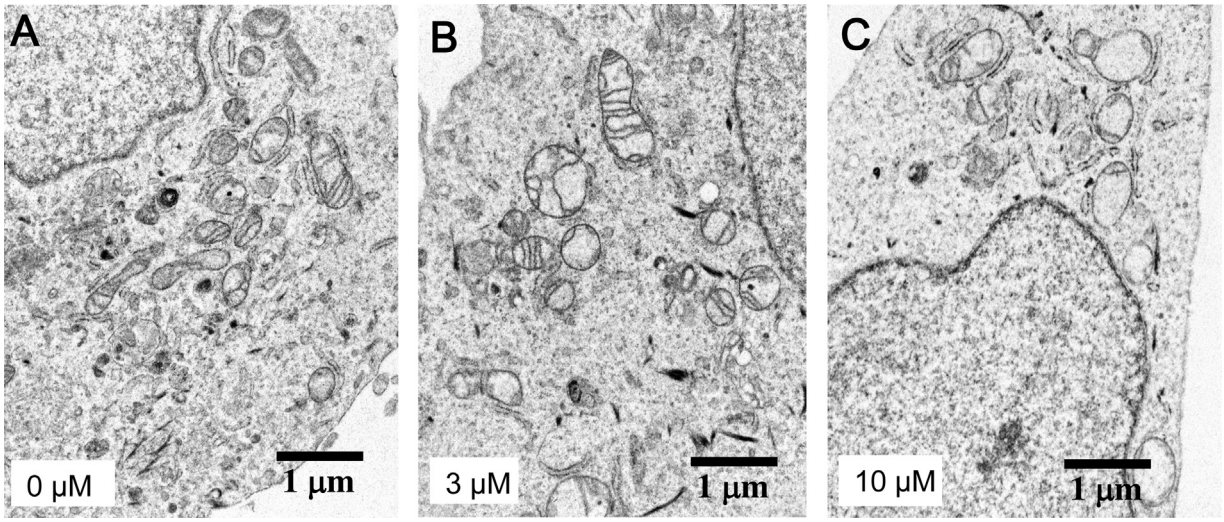

Fig. 3. Induction of mitochondrial vacuolization by compound **11**. Cells were treated for 3 h with 0 (control), 3 or 10 μM of compound **11**. After washing three times with 5 ml of cold PBS(−), the cells were fixed for 1 h with 2% glutaraldehyde and the fine cell structures were observed under TEM.

aqueous solution of isopropanol at 80 °C for 30 min) for anion analysis.

2.8.1. Cationic metabolite analysis

For cationic metabolite analysis using CE-TOFMS, sample separation was performed in fused silica capillaries (50 μm i.d. ×100 cm total length) filled with 1 M formic acid as the reference electrolyte. The capillary was flushed with formic acid (1 M) for 20 min before the first use and for 4 min before each sample injection. Sample solutions (approximately 3 nl) were injected at 50 mbar for 5 s and a voltage of 30 kV (constant voltage) was applied. The capillary temperature was maintained at 20 °C and the temperature of the sample tray was kept below 5 °C. The sheath liquid, composed of methanol/water (50% v/v) and 0.1 μM hexakis(2,2-difluoroethoxy) phosphazene (Hexakis), was delivered at 10 μl/min. ESI-TOF-MS was conducted in the positive ion mode. The capillary voltage was set at 4 kV and the flow rate of nitrogen gas (heater temperature = 300 °C) was set at 7 psig. In TOF-MS, the fragmentor, skimmer and OCT RF voltages were 75, 50 and 125 V, respectively. Automatic recalibration of each acquired spectrum was performed using reference standards ([^{13}C isotopic ion of protonated methanol dimer $(2MeOH+H)]^+$, m/z 66.0631) and ([protonated Hexakis $(M+H)]^+$, m/z 622.0290). Mass spectra were acquired at a rate of 1.5 cycles/s over a m/z range of 50–1000.

2.8.2. Anionic metabolite analysis

For anionic metabolite analysis using CE-TOF-MS, a commercially available COSMO(+) capillary (50 μm × 105 cm, Nacalai Tesque, Kyoto, Japan), chemically coated with a cationic polymer, was used for separation. Ammonium acetate solution (50 mM; pH 8.5) was used as the electrolyte for separation. Before the first use, the new capillary was flushed successively with the running electrolyte (pH 8.5), 50 mM acetic acid (pH 3.4), and then the electrolyte again for 10 min each. Before each injection, the capillary was equilibrated for 2 min by flushing with the acetic acid again and then with the running electrolyte for 5 min. A sample solution (approximately 30 nl) was injected at 50 mbar for 30 s, and a voltage of −30 kV was applied. The capillary temperature was maintained at 20 °C and the sample tray was cooled below 5 °C. An Agilent 1100 series pump equipped with a 1:100 splitter was used to deliver 10 μl/min of 5 mM ammonium acetate in 50% (v/v) methanol/water, containing 0.1 μM Hexakis, to the CE interface. Here, it was used as a sheath liquid surrounding the CE capillary to provide a stable electrical connection between the tip of the capillary and the grounded electrospray needle. ESI-TOF-MS was conducted in the negative ionization mode at a capillary voltage of 3.5 kV. For TOF-MS, the fragmentor, skimmer and OCT RF voltages were set at 100, 50 and 200 V, respectively. The flow rate of the drying nitrogen gas (heater temperature = 300 °C) was maintained at 7 psig. Automatic recalibration of each acquired spectrum was performed using reference standards ([^{13}C isotopic ion of deprotonated acetic acid dimer $(2CH_3COOH-H)]^-$, m/z 120.03841), and ([Hexakis deprotonated acetic acid $(M+CH_3COOH-H)]^-$, m/z 680.03554). Exact mass data were acquired at a rate of 1.5 spectra/s over a m/z range of 50–1000.

2.9. Statistical analysis

Data are expressed as the mean ± standard deviation (SD). Statistical analysis was performed by paired t-test. Differences were considered significant at $p<0.05$. Raw data of metabolomics analysis were analyzed using our proprietary software, MasterHands [23]. The processing flow used in this software was the noise-filtering, baseline correction, peak detection and integration of the peak area from sliced electropherograms (the width of each electropherogram was 0.02 m/z), elimination of noise and redundant features, and generation of an aligned data matrix with annotated metabolite identities and relative areas (peak areas normalized to those of internal standards) [24].

Concentrations were calculated using external standards based on relative area, i.e., the area divided by the area of the internal standards. Overall metabolomic profiles were accessed by principal component (PC) analysis (PCA) (Supplementary Figs. 1S and 2S). XLstat (Ver. 2014.1.04, Addinsoft, Paris, France) and GraphPad Prism (Ver 5.04, GraphPad Software, San Diego, CA) were used for PCA and other statistical tests. p-values calculated for metabolomic data were corrected by false discovery rate (FDR), accommodating multiple independent tests using R package (Ver. 3.0.2., http://www.r-project.org/) and corrected $p<0.05$ was considered significant. FDR (such as Q-value) was introduced as an indicator that shows to which extent the false positive is approved, since p-value alone produce many false positive due to multiple independent statistical tests for evaluating metabolomics data.

Internal standards were added to both test and standard samples to eliminate the systematic bias and absolute quantitation was performed by 1-point calibration curve using external

standards. Since injection volume of sample to CE was extremely small (approximately 3 nl) as compared with LC, we used 1-point calibration that keeps the linearity with negligible incidence of ion-suppression [22,25].

3. Results

3.1. Tumor-specificity

3-Styrylchromones (compounds **4**, **6**, **11**) showed weak cytotoxicity against human oral keratinocyte (HOK) (CC_{50} = 70, 77 and 19 μM) (E) and primary human gingival epithelial cells (HGEP) (CC_{50} = 178, 610 and >800 μM) (F), as compared with human OSCC cell lines (mean CC_{50} = 6.4, 13 and 2.0 μM) (B), yielding the tumor-specificity (TS) value of 10.9, 5.9, and 9.5 (E/B), and 27.8, 46.9 and >400 (F/B), respectively (Table 1). On the other hand, doxorubicin and 5-FU showed much higher cytotoxicities against both HOK (CC_{50} = 1.31 and 24.7 μM, respectively) (E) and HGEP cells (CC_{50} = 0.027 and 18.8 μM, respectively) (F), yielding very low tumor-specificities (1.4–8.7) (E/B) and (0.2–1.0) (F/B), respectively (Table 1). Taken together, these results demonstrated that 3-styrylchromones (compounds **4**, **6**, **11**) showed higher tumor-specificity, regardless of the type of normal cells: either epithelial or mesenchymal origin.

In order to identify which compounds have both good potency and selective toxicity to neoplasms, the potency-selectivity expression (PSE) values of the compounds were calculated. This property is the product of the reciprocal of the average CC_{50} value and the average TS figure multiplied by 100 [26]. When HGF/HPLF/HPC was used as normal cells, doxorubicin showed the highest PSE value (>17,333), followed by compound **11** (3450) > **4** (630) > 5-FU (>309) > **6** (200) (D/B^2 in Table 1). When HOK cells were used as normal cells, doxorubicin showed the highest PSE value (5800), followed by compound **11** (475) > **4** (170) > **6** (45) > 5-FU (7.8) (E/B^2 in Table 1). When HGEP cells were used as normal cells, compound **11** showed the highest PSE value (>20,000), followed by **4** (434) > **6** (361) > doxorubicin (133) > 5-FU (5.6) (F/B^2 in Table 1). These results showed that compound **11** has the highest potency and selective toxicity to neoplasms among these three 3-styrylchromones.

3.2. Time-course of cytotoxicity induction

We next performed the pulse-chase experiments with 3-styrylchromones to determine the minimum treatment time required for cytotoxicity induction. HSC-2 cells were treated for various times with increasing concentrations of compound **4**, **6** or **11**, and then cultured in drug-free medium until 47 h after treatment to determine the viable cell number. The magnitude of cytotoxicity induction by these drugs increased with treatment time up to 21 h (Exp. I in Table 2). Close inspection of the time kinetics demonstrated two plateaus of CC_{50} value at 3–6.7 h and 21–47 h after exposure. Repeated experiments reproduced similar results with two plateaus of CC_{50} value at 3–7 h and 23–47 h (Exp. II in Table 2). Compound **11** showed the highest cytotoxicity [CC_{50} = <1.56 μM (Exp. I); <0.39 μM (Exp. II)], followed by compound **4** [CC_{50} = 2.5 μM (Exp.I); 2.6 μM (Exp. II)] and then compound **6** [CC_{50} = 5.1 μM (EXP. I); 4.2 μM (Exp. II)] (Table 1). The orders of cytotoxicity potencies of these 3 compounds were the same with that of our previous data [12]. It was unexpected that higher concentrations of compounds **4**, **11** were cytotoxic, producing more than 90% dead cells, whereas compound **6** was rather cytostatic, leaving 30% viable cells (Fig. 2). These data suggest that the cytotoxicity was triggered as early as 3 h after treatment with compound **11**, and **11** showed the highest cytotoxicity and tumor-specificity among three 3-styrylchromones.

Table 2
Time course of cytotoxicity induction by compounds **4**, **6** and **11**. HSC-2 cells were exposed for the indicated times with various concentrations of compound **4**, **6** or **11**, replaced with fresh culture medium without sample, and incubated until 47 h after addition of sample. The 50% cytotoxic concentration (CC_{50}) was determined from the dose–response curve described in Fig. 2.

	CC_{50} (μM)		
Exposure time (h)	[4]	[6]	[11]
Exp. I			
1	61	65	18
3	20	45	10
6.7	21	50	9.5
21	2.5	5.1	<1.56
31	2.4	4.5	<1.56
47	2.4	4.6	<1.56
Exp. II			
1	41	42	14
3	19	19	5.9
7	20	20	5.5
23	2.6	4.2	<0.39
31	3.9	4.7	<0.39
47	4.3	2.2	<0.39

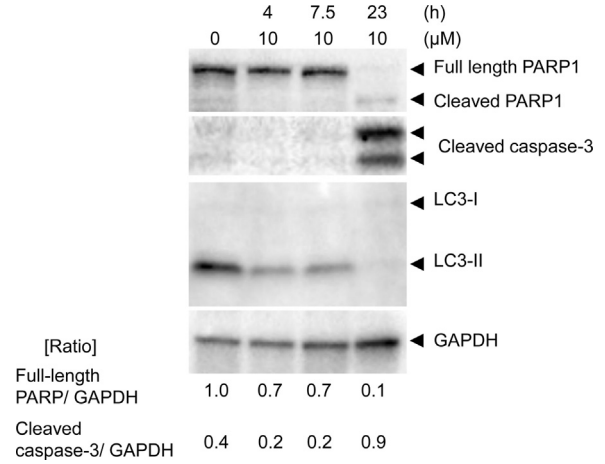

Fig. 4. Biological feature of compound **11**-induced cell death. A. Detection of the apoptotic marker, cleaved PARP1 and caspase-3, and the autophagic marker, LC3 in compound **11**-induced cell death. Cells were treated with or without 10 μM compound **11** for indicated time, and the cell lysates were analyzed by western blotting using anti-PARP, anti-caspase 3, anti-LC3, and anti-GAPDH antibodies. The expression of GAPDH was used as an internal control. Density of full-length PARP1 and cleaved caspase-3 proteins is represented by the ratio of full-length PARP1/GAPDH or cleaved caspase-3/GAPDH protein band in each time points.

3.3. Effect on fine cell structure

We next investigated the possible intracellular changes during early stages of cell cytotoxicity induction. When HSC-2 cells were treated for 3 h with 3 (B) or 10 (C) μM of compound **11**, mitochondrial vacuolization became prominent as compared with control cells (A) (Fig. 3), suggesting the induction of mitochondrial injury.

3.4. Type of cell death induced by compound 11

We investigated what type of cell death induced by compound **11** in HSC-2 cells, using cleavage of PARP1 and caspase-3, as apoptosis marker [27] and LC3 as autophagy marker [28] (Fig. 4). Untreated HSC-2 cells expressed higher levels of LC3-II than LC3-I, suggesting constitutional expression of autophagy marker (lane 1). When HSC-2 cells were incubated for 4, 7.5 and 23 h with 10 μM compound **11**,

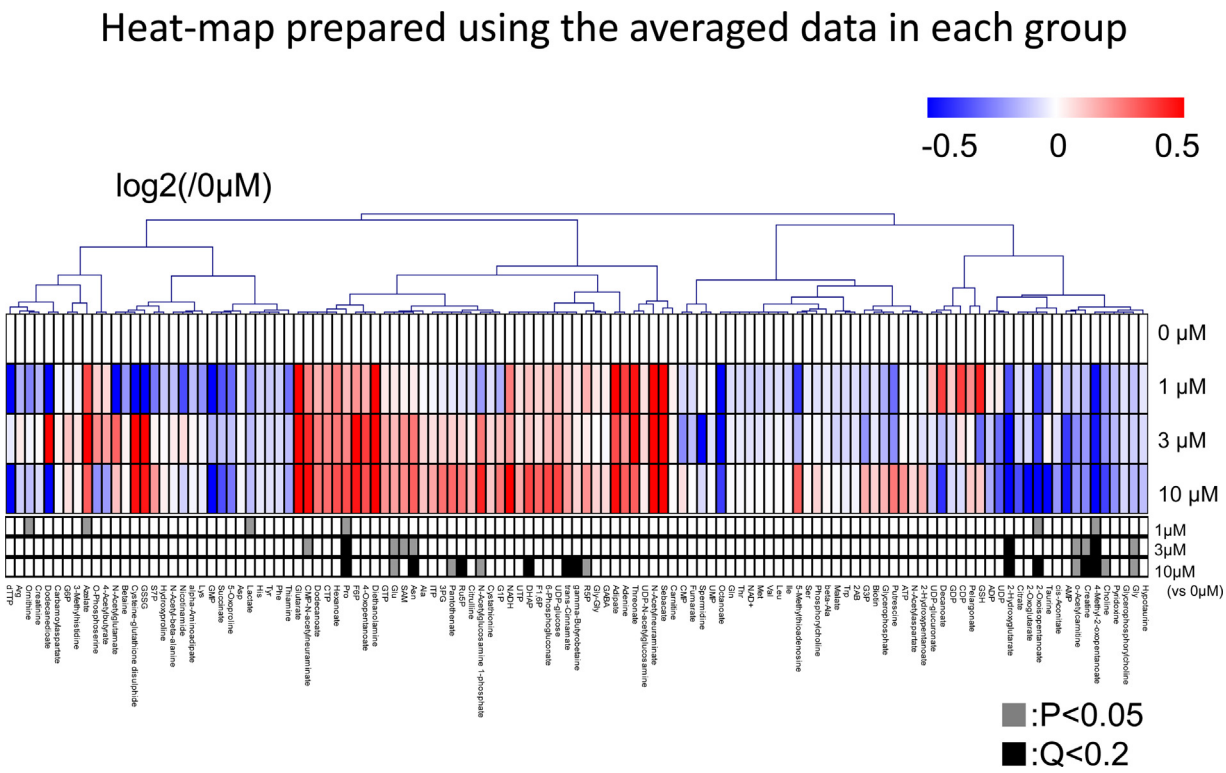

Fig. 5. Heat-map and bar graph visualization of the quantified metabolites. Heatmap showing the quantified metabolites using a white–blue–red scheme, and the fold-change of metabolites in 0, 1, 3 or 10 μM of compound **11**-treated cells. *Q* value is a *p* value corrected by FDR. (For interpretation of the references to color in this figure legend, the reader is referred to the web version of this article.)

the LC3-II expression decreased time-dependently to undetectable level (lane 2–4). This was paralleled with the loss of full length PARP at 23 h after treatment and the appearance of cleaved PARP1 and caspase-3 by limited digestion (lane 4). These results indicate that the treatment of compound **11** induced apoptotic cell death after suppression of autophagy.

It has recently been reported that benfotiamine induced paraptosis [characterized by cytoplasmic vacuolization and sensitivity to specific BH channel blocker (tetraethylammonium)] in leukemia cells without induction of apoptosis nor autophagy [29]. Therefore, there was a possibility that compound **11**, that induce mitochondrial vacuolization (Fig. 3), may induce paraptosis. This possibility, however, seems to be low, since we found that the cytotoxicity of **11** was not inhibited by BH blocker (tetraethylammonium) (Supplementary Fig. 3).

3.5. *Effect on metabolomic profiles*

HSC-2 cells were incubated for 3 h with 0 (control), 1, 3 or 10 μM compound **11** and intracellular metabolites were extracted with methanol and subjected to metabolomics analysis. A total of 119 metabolites were detected, and among that, 22 metabolites showed significant changes (Fig. 5). We identified these metabolites using standard mixtures. We confirmed that the corrected migration time, *m*/*z* value and distribution of isotopic peaks of each metabolite were identical with those of standard mixtures. We also performed spike test that confirmed that the addition of standard mixture to each sample resulted in the increase of peak that corresponds with each standard component.

Treatment of compound **11** did not significantly affect the intracellular concentration of metabolites in TCA cycle (citrate, *cis*-aconiate, succinate, fumarate, malate) (minor reduction), glycolytic metabolites (glucose-6-phosphate, fructose 6-phosphate, fructose 1,6-bisphospate, 3-phosphoglyceric acid) (minor increase), lactate (minor reduction), urea cycle (citrullin, arginine, ornithine) (no change or minor reduction) and polyamine pathway (putrescine, spermidine) (minor reduction) and the ratios of AMP/ATP (minor reduction), GMP/GTP (minor reduction) and NADH/NAD^+ ratio (minor increase) (Supplementary Table 1). We could not observe any significance to pathways/cycles/ratios, possibly due to the fact that metabolomics assay was performed at much earlier stages after treatment with compound **11** when apoptosis induction was not detected. Tracer experiments with precursor metabolites labeled with stable isotope are necessary to identify the target pathways/metabolites.

On the other hand, intracellular concentrations of 4-methyl-2-oxopentanoate, 2-hyroxyglutarate, creatine, 2-oxoisopentanoate ($Q < 0.2$), glycine (Gly) and choline ($p < 0.05$) were significantly reduced (Fig. 6A). 2-Oxogltarate was also reduced, but not significantly.

Intracellular concentrations of proline (Pro), asparagine (Asn), dihydroxyacetone phosphate (DHAP), ribulose 5 phosphate (Ru5P), transcinnamate, γ-butyrobetaine ($Q < 0.2$) and glutamic acid (Glu) ($p < 0.05$) were significantly increased (Fig. 6B). Diethanolamine and cytidine diphosphate-choline (CDP-choline) were also increased, but not significantly.

4. Discussion

The present study demonstrated that compound **11**, the most cytotoxic compound among three 3-styrylchromones, showed the highest tumor-specificity (TS = 9.5, >400), based on higher cytotoxicity against human OSCC cell lines, as compared with human epithelial normal oral cells HOK (TS = 9.5) and HGPE (TS > 400) (Table 1). It was unexpected that doxorubicin and 5-FU were extremely cytotoxic to HOK (TS = 1.4–8.7) and HGEP (TS = 0.2–1.0), giving disappointedly lower tumor selectivity. This may be resulted from the higher enhanced DNA replication

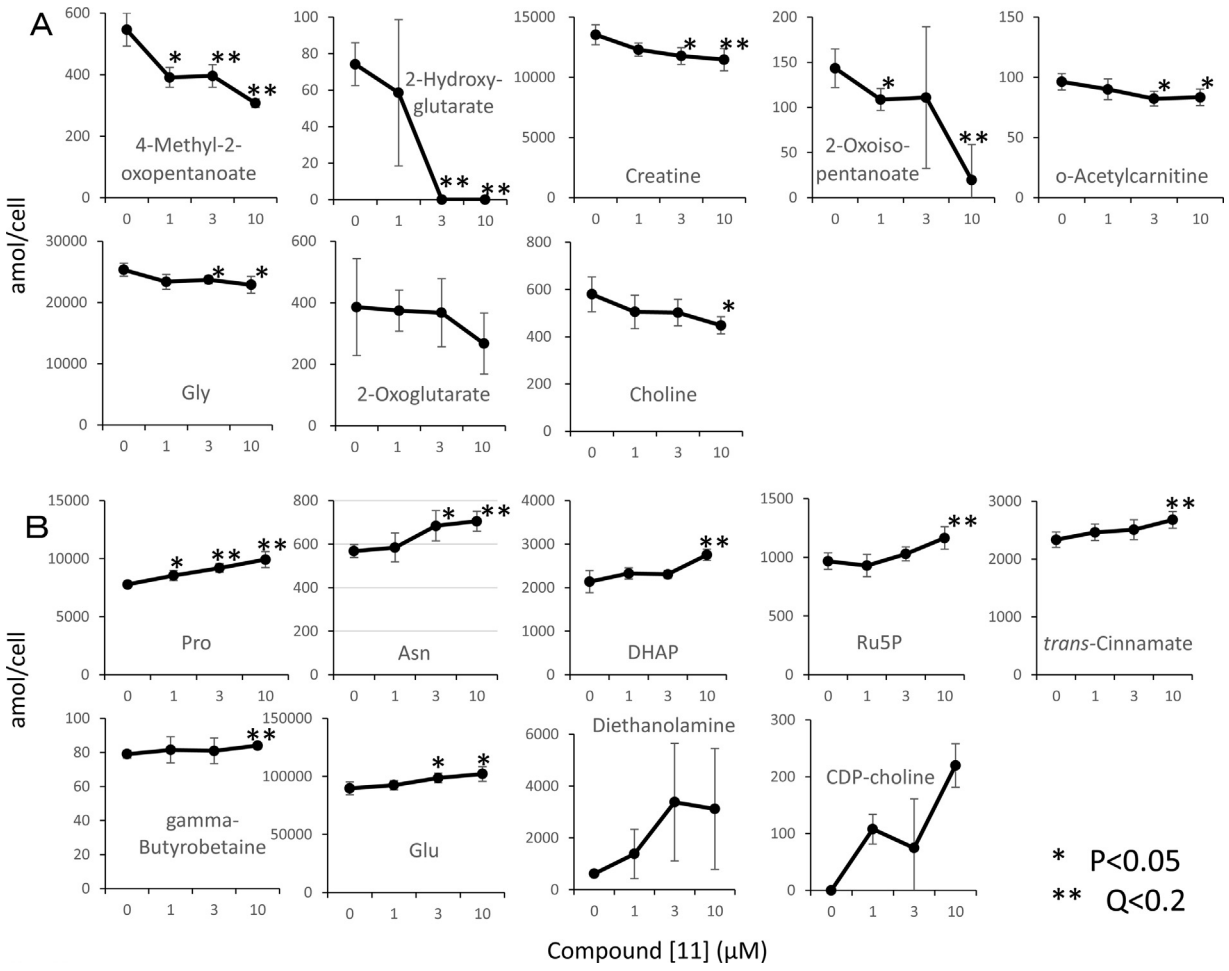

Fig. 6. Effects of compound **11** on various cellular compounds. HSC-2 cells were treated for 3 h with 0 (control), 1, 3 and 10 μM of compound **11**, and intracellular concentrations of 4-methyl-2-oxopentanoate, 2-hydroxyglutarate, creatine, 2-oxoisopentanoate, *o*-acetylcarnitine, glycine (Gly), 2-oxoglutarate, choline (A), proline (Pro), asparagine (Asn), dihydroxyacetone phosphate (DHAP), ribulose 5 phosphate (Ru5P), *trans*-cinnamate, γ-butyrobetaine, glutamic acid (Glu), diethanolamine and CDP-choline (B) were determined by metabolomics analysis. Each value represents mean ± S.D. of quadruplicate assays. *Q* value is a *p* value corrected by FDR.

activities of HOK and HGEP cells by growth factor-enriched medium, supplied by manufacturers. Although the cytotoxicity of doxorubicin may be partially reduced by stimulating the basal mitochondrial respiration [30], special care should be taken for oral application of these antineoplastic agents. Since compound **11** had comparable hydrophobic property ($\log P = 3.10$) with doxorubicin ($\log P = 2.82$), the higher tumor-specificity of 3-styrylchromones cannot simply be explained by its hydrophobic property.

We next investigated what are the earliest intracellular changes induced by compound **11**. The pulse-chase experiments revealed that 3 h-treatment time with compound **11** committed the cells into the first wave of cell death pathway (Table 2). TEM showed that compound **11** dose-dependently induced mitochondrial vacuolization, suggesting the mitochondrial injury at early stage of cell death induction. Interestingly, Western blot analysis revealed that HSC-2 cells constitutionally expressed higher level of autophagy marker LC3-II, and treatment of compound **11** initially induced the loss of autophagy marker, followed by appearance of apoptosis marker (cleaved PARP1 and caspase-3) at later stage (Fig. 4). These data suggest that the initial reduction of autophagy, which that is involved in cell survival, triggered apoptosis. Constitutional expression of LC3-II in HSC-2 cells may explain why many anticancer agents, such as doxorubicin [31], mitomycin C [32], gefitinib in combination with docetaxel [33], were hard to induce typical apoptosis in this cell line.

Metabolomic analysis demonstrated that compound **11** did not significantly affect major cellular metabolic pathways such as TCA cycle, glycolysis, urea and polyamine pathways, nor effected the ATP and GTP utilization. Compound **11**, however, significantly reduced the intracellular concentrations of 4-methyl-2-oxopentanoate and 2-oxoisopentanoate that are the degradation products of leucine and valine (catalyzed by branched-chain-amino acid amino transferase EC2.6.1.42), respectively (Fig. 6A). Compound **11** also reduced the intracellular concentrations of 2-hydroxyglutarate and creatine, possibly due to the decline of 2-oxoglutarate (catalyzed by 2-hydroxyglutarate dehydrogenase EC 1.1.99.2) and glycine (Gly) (catalyzed by arginine glycine amidinotransferase EC2.1.4.1 and guanidinoacetate *N*-methyltransferase EC2.1.2.1), respectively. On the other hand, Compound **11** significantly increased the intracellular concentrations of proline (Pro), asparagine (Asn), dihydroxyacetone phosphate (DHAP), ribulose 5 phosphate (Ru5P), transcinnamate, γ-butyrobetaine and glutamic acid (Glu) (Fig. 6B). It should be noted that the only amino acid significantly changed were Pro, Gly, and Asn. We have recently found that salivary concentrations of Gly and Pro were age-dependently increased keeping the constant ratio of Gly to Pro [34] (Sugimoto et al; unpublished data). However, biological significance of these changes is not clear at present.

We also found that compound **11** dramatically but not significantly increased the intracellular concentration of diethanolamine. Large standard deviation of intracellular levels of diethanolamine

diminished the statistical significance. This suggests the rapid turnover of this compound, rather the experimental artifacts. As far as we know, the cytotoxicity of diethanolamine have not been well investigated, and most of previous studies have limited to non-human creatures such as aquatic biota [35]. Treatment of cultured mouse neural precursor cells with diethanolamine reduced the intracellular uptake and accumulation of choline [36]. When pregnant mice were treated dermally with diethanolamine, apoptosis was induced in the hippocampal ventricular zone of the brain of fetuses [37]. This agrees with the present finding that compound **11** increased the intracellular levels of diethanolamine and CDP-choline (Fig. 6B) and reduced that of choline (Fig. 6A). This suggests that compound **11** down-regulate the glycerophospholipid pathway. The relatively higher lipophilic property of diethanolamine ($\log P = 1.761$) suggests its interaction with lipophilic membrane components. Since the extracellular concentration of diethanolamine was not apparently changed before and after treatment with compound **11** (12.1 ± 13.4 μM and 11.8 ± 5.3 μM, respectively) (Supplementary Table S1), the increase of diethanolamine should be the increase of its production, rather than the entry from the medium. There are many factors that may affect the fluctuations of diethanolamine level; type of cells and inducers. During NaF-induced apoptosis-induction in HSC-2 cells, we have found similar elevation of diethanolamine (our preliminary observation). However, the connection of diethanolamine and apoptosis induction awaits more rigorous time course study. Further studies are needed to elucidate the mechanism by which compound **11** increases diethanolamine level.

Our recent metabolomics analysis demonstrated that (i) apoptosis induction (characterized by caspase-3 activation, internucleosomal DNA fragmentation, enhanced BAD protein expression) by NaF (5 mM, 4 h) in HSC-2 cells [38] was accompanied by rapid decline of glycolysis and TCA cycle progression and increase of ATP utilization (AMP/ATP ratio) and oxidative stress (elevated level of GSSG/GSH ratio, methionine sulfoxide) [17], and (ii) necrosis-induction by eugenol (1.4 mM, 4 h) in HSC-2 cells was accompanied by slight enhancement of glycolysis and oxidative stress without apparent change in TCA cycle and ATP utilization [15], and (iii) necrosis-induction by eugenol (2 mM, 20 min) in human normal gingival fibroblast, periodontal ligament fibroblast and pulp cells was accompanied by rapid decline of TCA cycle without affecting glycolysis (Sakagami et al., manuscript in preparation). These data suggest possible connection between the apoptosis induction and ATP utilization, and that perturbation of glycolysis and TCA cycle, and oxidative stress are not specific for the type of cell death. On the other hand, we have not observed the increase of ATP utilization at 3 h after treatment with compound **11**, when apoptosis induction was not detected. Further time course study is essential to connect ATP utilization and apoptosis more accurately.

We found that pretreatment with cycloheximide inhibited the cytotoxicity (Supplementary Fig. 3) and morphological changes (i.e., displaying round shape and detachment from the plastic plate) (data not shown) induced by compounds **4**, **6** and **11**, suggesting that protein synthesis may be required for cytotoxicity induction.

Compound **11** is not only a new compound that shows the highest TS and PSE values among three 3-styrylchromones, but also its structure can be modified by introduction of various substituent groups at 5–7 position of chromone ring. Further studies are needed to investigate whether such substituted compounds have higher tumor-specificity than the parent compound.

Our recent QSAR analysis of sixteen 3-styryl-2*H*-chromene derivatives demonstrated that all derivatives showed relatively high tumor selectivity. Especially, compound that have a methoxy group at 7-position of the chromene ring and chlorine at 4′-position of phenyl group in styryl moiety showed the highest tumor-specificity (TS) and potency-selectivity expression (PSE) values, exceeding those of resveratrol, doxorubicin and 5-FU [39]. These data, combined with the present study, suggest the possible antitumor potential of 3-styryl-4*H*-chromones and 3-styryl-2*H*-chromenes.

Since at least 10^6 cells are required for each time point, no one has succeeded to perform the metabolomic analysis at a time point of the cell cycle, under strictly controlled conditions. If more sensitive method would be established, cell cycle effects could be accurately evaluated and subtracted.

Acknowledgements

We are very grateful to Prof. Kaoru Kusama for his suggestion and interpretation of the data. This work was supported by Grant-in-Aid for Challenging Exploratory Research from The Ministry of Education, Culture, Sports, Science and Technology (Sakagami H. 25670897), research funds from Meikai University School of Dentistry and a research funds from the Yamagata Prefectural Government and Tsuruoka City, Japan.

Appendix A. Supplementary data

Supplementary data associated with this article can be found, in the online version, at http://dx.doi.org/10.1016/j.toxrep.2015.09.009.

References

[1] A. Gomes, E. Fernandes, A.M.S. Silva, C.M.M. Santos, D.C.G.A. Pinto, J.A.S. Cavaleiro, J.L.F.C. Lima, 2-Styrylchromones: novel strong scavengers of reactive oxygen and nitrogen species, Bioorg. Med. Chem. 15 (2007) 6027–6036.
[2] G. Doria, C. Romeo, A. Forgione, P. Sberze, N. Tibolla, M.L. Corno, G. Cruzzola, G. Cadelli, Antiallergic agents. III: substituted *trans*-2-ethenyl-4-oxo-4*H*-benzopyran-6-carboxylic acids, Eur. J. Med. Chem. 14 (1979) (1979) 347–351.
[3] A. Gomes, E. Fernandes, A.M.S. Silva, D.C.G.A. Pinto, C.M.M. Santos, J.A.S. Cavaleiro, J.L.F.C. Lima, Anti-inflammatory potential of 2-styrylchromones regarding their interference with arachidonic acid metabolic pathways, Biochem. Pharmacol. 78 (2009) 171–177.
[4] K. Momoi, Y. Sugita, M. Ishihara, K. Satoh, H. Kikuchi, K. Hashimoto, I. Yokoe, H. Nishikawa, S. Fujisawa, H. Sakagami, Cytotoxic activity of styrylchromones against human tumor cell lines, In Vivo 19 (2005) 157–163.
[5] J. Marinho, M. Pedro, D.C.G.A. Pinto, A.M.S. Silva, J.A.S. Cavaleiro, C.E. Sunkel, M.S.J. Nascimento, 4′-methoxy-2-styrylchromone a novel microtubule-stabilizing antimitotic agent, Biochem. Pharmacol. 75 (2008) 826–835.
[6] A.Y. Shaw, C.Y. Chang, H.H. Liau, P.J. Lu, H.L. Chen, C.N. Yang, H.Y. Li, Synthesis of 2-styrylchromones as a novel class of antiproliferative agents targeting carcinoma cells, Eur. J. Med. Chem. 44 (2009) 2552–2562.
[7] N. Desideri, P. Mastromarino, C. Conti, Synthesis and evaluation of antirhinovirus activity of 3-hydroxy and 3-methoxy 2-styrylchromones, Antivir. Chem. Chemother. 14 (2003) 195–203.
[8] C. Conti, P. Mastromarino, P. Goldoni, G. Portalone, N. Desideri, Synthesis and anti-rhinovirus properties of fluoro-substituted flavonoids, Antivir. Chem. Chemother. 16 (2005) 267–276.
[9] C. Conti, N. Desideri, New 4*H*-chromen-4-one and 2*H*-chromene derivatives as anti-picornavirus capsid-binders, Bioorg. Med. Chem. 18 (2010) 6480–6488.
[10] V.L.M. Silva, A.M.S. Silva, D.C.G.A. Pinto, J.A.S. Cavaleiro, A. Vasas, T. Patonay, Synthesis of (*E*)- and (*Z*)-3-styrylchromones, Monatsh. Chem. 139 (2008) 1307–1315.
[11] K. Takao, R. Ishikawa, Y. Sugita, Synthesis and biological evaluation of 3-styrylchromone derivatives as free radical scavengers and α-glucosidase inhibitors, Chem. Pharm. Bull. 62 (2014) 810–815.
[12] C. Shimada, Y. Uesawa, R. Ishii-Nozawa, M. Ishihara, H. Kagaya, T. Kanamto, S. Terakubo, H. Nakashima, K. Takao, Y. Sugita, H. Sakagami, Quantitative structure–cytotoxicity relationship of 3-styrylchromones, Anticancer Res. 34 (2014) 5405–5412.
[13] K. Kantoh, M. Ono, Y. Nakamura, Y. Nakamura, K. Hashimoto, H. Sakagami, H. Wakabayashi, Hormetic and anti-radiation effects of tropolone-related compounds, In Vivo 24 (2010) 843–852.
[14] R. Garcia-Contreras, R.J. Scougall-Vilchis, R. Contreras-Bulnes, Y. Kanda, H. Nakajima, H. Sakagami, Effects of TiO_2 nano glass ionomer cements against normal and cancer oral cells, In Vivo 28 (2014) 895–907.
[15] T. Koh, Y. Murakami, S. Tanaka, M. Machino, H. Onuma, M. Kaneko, M. Sugimoto, T. Soga, M. Tomita, H. Sakagami, Changes of metabolic profiles in

an oral squamous cell carcinoma cell line induced by eugenol, In Vivo 27 (2013) 233–244.
[16] A. Hirayama, M. Sugimoto, A. Suzuki, Y. Hatakeyama, A. Enomoto, S. Harada, T. Soga, M. Tomita, T. Takebayashi, Effects of processing and storage conditions on charged metabolomic profiles in blood, Electrophoresis (2015), http://dx.doi.org/10.1002/elps.201400600 [Epub ahead of print].
[17] H. Sakagami, M. Sugimoto, S. Tanaka, H. Onuma, S. Ota, M. Kaneko, T. Soga, M. Tomita, Metabolomic profiling of sodium fluoride-induced cytotoxicity in an oral squamous cell carcinoma cell line, Metabolomics 10 (2014) 270–279.
[18] R. Garcia-Contreras, M. Susigmoto, N. Umemura, M. Kaneko, Y. Hatakeyama, T. Soga, M. Tomita, R.J. Scougall-Vilchis, R. Contreras-Bulnes, H. Nakajima, H. Sakagami, Alteration of metabolomic profiles by titanium dioxide nanoparticles in human gingivitis model, Biomaterials 57 (2015) 33–40.
[19] M. Sugimoto, M. Kawakami, M. Robert, T. Soga, M. Tomita, Bioinformatics tools for mass spectroscopy-based metabolomic data processing and analysis, Curr. Bioinform. 7 (2012) 96–108.
[20] T. Soga, R. Baran, M. Suematsu, Y. Ueno, S. Ikeda, T. Sakurakawa, Y. Kakazu, T. Ishikawa, T. Robert, T. Nishioka, M. Tomita, Differential metabolomics reveals ophthalmic acid as an oxidative stress biomarker indicating hepatic glutathione consumption, J. Biol. Chem. 281 (2006) 16768–16776.
[21] M. Sugimoto, H. Sakagami, Y. Yokote, H. Onuma, M. Kaneko, M. Mori, Y. Sakaguchi, T. Soga, M. Tomita, Non-targeted metabolite profiling in activated macrophage secretion, Metabolomics 8 (2012) 624–633.
[22] T. Soga, K. Igarashi, C. Ito, K. Mizobuchi, H.P. Zimmermann, M. Tomita, Metabolomic profiling of anionic metabolites by capillary electrophoresis mass spectrometry, Anal. Chem. 81 (15) (2009) 6165–6174.
[23] M. Sugimoto, D.T. Wong, A. Hirayama, T. Soga, M. Tomita, Capillary electrophoresis mass spectrometry-based saliva metabolomics identified oral, breast and pancreatic cancer-specific profiles, Metabolomics 6 (2010) 78–95.
[24] M. Sugimoto, M. Kawakami, M. Robert, T. Soga, M. Tomita, Bioinformatics tools for mass spectroscopy-based metabolomic data processing and analysis, Curr. Bioinform. 7 (2012) 96–108.
[25] T. Soga, Y. Ohashi, Y. Ueno, H. Naraoka, M. Tomita, T. Nishioka, Quantitative metabolome analysis using capillary electrophoresis mass spectrometry, J. Proteome Res. 2 (2003) 488–494.
[26] S. Das, U. Das, H. Sakagami, N. Umemura, S. Iwamato, T. Matsuta, M. Kawase, J. Molnar, J. Serly, D.K.J. Gorecki, J.R. Dimmock, Dimeric 3,5-bis(benzylidene)-4-piperidones: a novel cluster of tumour-selective cytotoxins possessing multidrug-resistant properties, Eur. J. Med. Chem. 51 (2012) 193–199.
[27] F.J. Oliver, G. de la Rubia, V. Rolli, M.C. Ruiz-Ruiz, G. de Murcia, J.M. Murcia, Importance of poly(ADP-ribose) polymerase and its cleavage in apoptosis. Lesson from an uncleavable mutant, J. Biol. Chem. 273 (50) (1998) 33533–33539.
[28] Y. Kabeya, N. Mizushima, T. Ueno, A. Yamamoto, T. Kirisako, T. Noda, E. Kominami, Y. Ohsumi, T. Yoshimori, LC3, a mammalian homologue of yeast Apg8p, is localized in autophagosome membranes after processing, EMBO J. 19 (21) (2000) 5720–5728.
[29] N. Sugimori, J.L. Espinoza, L.Q. Trung, A. Takami, Y. Kondo, D.T. An, M. Sasaki, T. Wakayama, S. Nakao, Paraptosis cell death induction by the thiamine analog benfotiamine in leukemia cells, PLoS One 10 (4) (2015) e0120709, http://dx.doi.org/10.1371/journal.pone.0120709, eCollection.
[30] C.M. Deusa, C. Zehowskib, K. Nordgrenb, K.B. Wallaceb, A. Skildumb, P.J. Oliveiraa, Stimulating basal mitochondrial respiration decreases doxorubicin apoptotic signaling in H9c2 cardiomyoblasts, Toxicology 334 (2015) 1–11.
[31] F. Suzuki, K. Hashimoto, H. Kikuchi, H. Nishikawa, H. Matsumoto, J. Shimada, M. Kawase, K. Sunaga, T. Tsuda, K. Satoh, H. Sakagami, Induction of tumor-specific cytotoxicity and apoptosis by doxorubicin, Anticancer Res. 25 (2005) 887–893.
[32] M. Sasaki, M. Okamura, A. Ideo, J. Shimada, F. Suzuki, M. Ishihara, H. Kikuchi, Y. Kanda, S. Kunii, H. Sakagami, Re-evaluation of tumor-specific cytotoxicity of mitomycin C, bleomycin and peplomycin, Anticancer Res. 26 (2006) 3373–3380.
[33] Q. Chu, O. Amano, Y. Kanda, S. Kunii, Q. Wang, H. Sakagami, Tumor-specific cytotoxicity and type of cell death induced by gefitinib in oral squamous cell carcinoma cell lines, Anticancer Res. 29 (2009) 5023–5031.
[34] S. Tanaka, M. Machino, S. Akita, Y. Yokote, H. Sakagami, Changes in salivary amino acid composition during aging, In Vivo 24 (2010) 853–856.
[35] J.L. Zurita, G. Repetto, A. Jos, A. Del Peso, M. Salguero, M. Lópes-Artiguez, D. Olano, A. Cameán, Ecotoxicological evaluation of diethanolamine using a battery of microbiotests, Toxicol. In Vitro 19 (2005) 879–886.
[36] M.D. Nickescu, R. Wu, A. Guo, K.A. de Costa, S.H. Zeisel, Diethanolamine alters proliferation and choline metabolism in mouse neural precursor cells, Toxicol. Sci. 96 (2007) 321–326.
[37] C.N. Craciunescu, R. Wu, S.H. Zeisel, Diethanolamine alters neurogenesis and induces apoptosis in fetal mouse hippocampus, FASEB J. 20 (2006) 1635–1640.
[38] S. Otsuki, K. Sugiyama, O. Amano, T. Yasui, H. Sakagami, Negative regulation of NaF-induced apoptosis by bad-CAII complex, Toxicology 287 (2011) 131–136.
[39] Y. Uesawa, H. Sakagami, M. Ishihara, H. Kagaya, T. Kanamoto, S. Terakubo, H. Nakashima, H. Yahagi, K. Takao, Y. Sugita, Quantitative structure-cytotoxicity relationship of 3-styryl-2*H*-chromenes, Anticancer Res. 35 (2015) 5299–5308.